



# Investigation of short-term effective radiative forcing of fire aerosols over North America using nudged hindcast ensembles

Yawen Liu<sup>1,2</sup>, Kai Zhang<sup>2</sup>, Yun Qian<sup>2</sup>, Yuhang Wang<sup>3</sup>, Yufei Zou<sup>3</sup>, Yongjia Song<sup>3</sup>, Hui Wan<sup>2</sup>, Xiaohong Liu<sup>4</sup>, and Xiu-Qun Yang<sup>1</sup>

<sup>1</sup>School of Atmospheric Sciences, Nanjing University, Nanjing, China

<sup>2</sup>Pacific Northwest National Laboratory, Richland, Washington, USA

<sup>3</sup>School of Earth and Atmospheric Sciences, Georgia Institute of Technology, Atlanta, Georgia, USA

<sup>4</sup>Department of Atmospheric Science, University of Wyoming, Laramie, Wyoming, USA

**Correspondence:** Yun Qian (yun.qian@pnnl.gov) and Xiu-Qun Yang (xqyang@nju.edu.cn)

Received: 3 May 2017 – Discussion started: 7 June 2017

Revised: 29 September 2017 – Accepted: 8 November 2017 – Published: 3 January 2018

**Abstract.** Aerosols from fire emissions can potentially have large impact on clouds and radiation. However, fire aerosol sources are often intermittent, and their effect on weather and climate is difficult to quantify. Here we investigated the short-term effective radiative forcing of fire aerosols using the global aerosol–climate model Community Atmosphere Model version 5 (CAM5). Different from previous studies, we used nudged hindcast ensembles to quantify the forcing uncertainty due to the chaotic response to small perturbations in the atmosphere state. Daily mean emissions from three fire inventories were used to consider the uncertainty in emission strength and injection heights. The simulated aerosol optical depth (AOD) and mass concentrations were evaluated against in situ measurements and reanalysis data. Overall, the results show the model has reasonably good predicting skills. Short (10-day) nudged ensemble simulations were then performed with and without fire emissions to estimate the effective radiative forcing. Results show fire aerosols have large effects on both liquid and ice clouds over the two selected regions in April 2009. Ensemble mean results show strong negative shortwave cloud radiative effect (SCRE) over almost the entirety of southern Mexico, with a 10-day regional mean value of  $-3.0 \text{ W m}^{-2}$ . Over the central US, the SCRE is positive in the north but negative in the south, and the regional mean SCRE is small ( $-0.56 \text{ W m}^{-2}$ ). For the 10-day average, we found a large ensemble spread of regional mean shortwave cloud radiative effect over southern Mexico (15.6 % of the corresponding ensemble mean) and the central US (64.3 %), despite the regional mean AOD time series being almost in-

distinguishable during the 10-day period. Moreover, the ensemble spread is much larger when using daily averages instead of 10-day averages. This demonstrates the importance of using a large ensemble of simulations to estimate the short-term aerosol effective radiative forcing.

## 1 Introduction

Natural and human-induced fires play an important role in the Earth system. Aerosol and gas emissions from biomass burning can change the atmospheric composition and potentially affect the weather and climate. Over 30 % of the global total emission of black carbon (BC) comes from open burning of forests, grasslands, and agricultural residues (Bond et al., 2013). For organic aerosols, substantial increases of concentrations dominated by organic carbon enhancements are observed in regions with biomass burning events (Zeng and Wang, 2011; Lin et al., 2013; Brito et al., 2014; Reddington et al., 2014). As a result, biomass burning emissions have a large impact on the global and regional mean aerosol optical depth (AOD; Jacobson, 2014).

Through interactions with radiation and cloud, fire aerosols can significantly affect Earth's long-term energy budget. Previous studies have investigated the global and regional radiative forcing of fire aerosols using long climatological simulations or satellite retrievals. For example, Ward et al. (2012) investigated the radiative forcing of global fires in preindustrial, present-day, and future periods. For

the present-day condition, they estimated a direct aerosol effect (or radiative forcing through aerosol–radiation interactions as defined in the IPCC Fifth Assessment Report (AR5),  $R_{\text{Fari}}$ ; see Sect. 2.4) of  $+0.1 \text{ W m}^{-2}$  and an indirect effect (radiative forcing through aerosol–cloud interactions,  $R_{\text{Faci}}$ ) of  $-1.0 \text{ W m}^{-2}$ . Using a newer model, Jiang et al. (2016) found similar  $R_{\text{Fari}}$  but slightly smaller  $R_{\text{Faci}}$  ( $-0.70 \text{ W m}^{-2}$ ). Sena et al. (2013) assessed the direct impact of biomass burning aerosols over the Amazon Basin using satellite data. Over the 10-year study period, the estimated radiative forcing is about  $-5.6 \text{ W m}^{-2}$ .

On short timescales, fire aerosols have even larger radiative impacts. Observed maximum daily direct aerosol radiative effects can reach  $-20 \text{ W m}^{-2}$  at the top of the atmosphere (TOA) locally in Amazonia during biomass burning seasons (Sena et al., 2013). Very large direct effects of fire aerosols have been observed during extreme fire events over central Russia (Tarasova et al., 2004; Chubarova et al., 2008, 2012). Instantaneous direct radiative effects (DREs) of emitted aerosols reached  $-167 \text{ W m}^{-2}$ , and monthly mean DREs reached about  $-65 \text{ W m}^{-2}$  in the 2010 Russia wildfires (Chubarova et al., 2012). Kolusu et al. (2015) investigated DRE of biomass burning aerosols over tropical South America. By quantifying results from the first and second day of 2-day single-member forecasts in September 2012, they found the modeled biomass burning aerosols reduced all-sky net radiation by  $8 \text{ W m}^{-2}$  at TOA and  $15 \text{ W m}^{-2}$  at the surface. The fire aerosol indirect effect may also significantly affect the cloud formation and radiative balance on short timescales. Using satellite data and a radiative transfer model, Kaufman et al. (2005) found an indirect radiative effect of  $-9.5 \text{ W m}^{-2}$  due to smoke-aerosol-induced cloud changes over the eastern South Atlantic for the 3-month period studied. Smoke-derived cloud albedo effect on local shortwave radiative forcing is estimated to be between  $-2$  and  $-4 \text{ W m}^{-2}$  in a day case study of aircraft-measured indirect cloud effects (Zamora et al., 2016).

Previous modeling studies on the short-term fire aerosol effects mainly focused on aerosol direct effects (e.g., Keil and Haywood, 2003; Chen et al., 2014; Kolusu et al., 2015), and only a couple of studies have investigated the indirect effects of fire aerosols (Lu and Sokolik, 2013). In addition, to estimate the aerosol indirect effect, long simulations (multi-year,  $> 5$  years preferred) are often needed to remove the noise, because aerosol life cycle and cloud properties are affected by strong natural variability on different timescales (Bony et al., 2006; Kooperman et al., 2012). To solve the problem, alternative methods have been proposed to help extract signals with shorter simulations. For example, nudging (also called Newton relaxation method) can help reduce uncertainties associated with natural variability by constraining certain meteorological fields towards prescribed conditions. A robust estimate of global anthropogenic aerosol indirect effects can be obtained on substantially shorter timescales (1–2 years) by implementing nudging to constrain simula-

tions with preindustrial and present-day aerosol emissions toward identical circulation and meteorology (Kooperman et al., 2012). When nudging towards reanalysis data, K. Zhang et al. (2014) found that constraining only the horizontal winds is a preferred strategy to estimate the aerosol indirect effect since it provides well-constrained meteorology without strongly perturbing the model's mean climate state. Another example is the use of representative ensembles of short simulations to replace a typical long integration. Wan et al. (2014) explored the feasibility of this method and showed that 3-day ensembles of 20 to 50 members are able to reveal the main signals revealed by traditional 5-year simulations.

In this study, we performed month-long and 10-day nudged Community Atmosphere Model version 5 (CAM5) simulations to investigate the effects of fire aerosols on radiation and cloud processes on short timescales (less than 2 weeks). Horizontal winds were nudged towards 6-hourly reanalysis to constrain the large-scale circulation and to allow for more accurate model evaluations against observations. We also used daily mean emissions from three fire inventories to consider the uncertainty in emission strength and injection heights. Even for short simulations, small perturbations of meteorological states might have large impact on the local aerosol and cloud properties, thus bringing uncertainty to the aerosol forcing estimate. Therefore, in our simulations, we also employed very weak temperature nudging ( $\sim 10$  days) in combination with ensembles to quantify the uncertainty. More details of the nudging setup are described in Sect. 2.3.

The rest of the paper is organized as follows. Section 2 describes the model and data used in this study. It also introduces how the ensembles are generated in the short nudged simulations and explains how the fire aerosol forcing is estimated. Results and discussions are presented in Sect. 3, and conclusions are summarized in Sect. 4.

## 2 Model, method, and data

### 2.1 Model description

In this study, we used the CAM version 5.3 with the finite-volume dynamical core at  $1.9^\circ$  (latitude)  $\times$   $2.5^\circ$  (longitude) horizontal resolution with 30 vertical layers. The aerosol life cycle is represented using the modal aerosol module MAM3 (Liu et al., 2012). CAM5 links the simulated aerosol fields with cloud and radiation through interactions of the aerosol module with the cloud microphysics and radiative transfer parameterizations. The two-moment bulk cloud microphysics scheme from Morrison and Gettelman (2008) is used to track mass mixing ratios and number concentrations of cloud droplets and ice crystals in stratiform clouds. Representation of shallow convection is based on the work of Park and Bretherton (2009). The deep-convection parameterization was developed by Zhang and McFarlane (1995)

and later revised by Richter and Rasch (2008) and Neale et al. (2008). Longwave and shortwave radiative transfer is calculated with the Rapid Radiative Transfer Model for GCMs (RRTMG; Mlawer et al., 1997; Iacono et al., 2008).

## 2.2 Fire emission inventories

Three fire emission inventories were used in this study. Two of them are widely used bottom-up inventories – Global Fire Emissions Database version 3.1 (GFED v3.1; van der Werf et al., 2010; [https://daac.ornl.gov/cgi-bin/dsviewer.pl?ds\\_id=1191](https://daac.ornl.gov/cgi-bin/dsviewer.pl?ds_id=1191)) and GFED v4.1s (Giglio et al., 2013; Randerson et al., 2012; [https://daac.ornl.gov/VEGETATION/guides/fire\\_emissions\\_v4.html](https://daac.ornl.gov/VEGETATION/guides/fire_emissions_v4.html)). Another one is a top-down emission inventory – Quick Fire Emissions Dataset version 2.4 (QFED v2.4). GFEDv3.1 and GFEDv4.1s provide global monthly emission at  $0.5^\circ \times 0.5^\circ$  and  $0.25^\circ \times 0.25^\circ$  spatial resolution, respectively, from 1997 through the present. Daily emission data can be obtained by disaggregating monthly emissions based on daily temporal variability in fire emissions derived from Moderate Resolution Imaging Spectroradiometer (MODIS) measurements of active fires (Mu et al., 2011). The daily emission data are obtained using daily scalars (<http://www.globalfiredata.org/data.html>) to distribute monthly emissions over the days and are only available from 2003 onwards. The more recent version, GFED v4.1s, improves by including small fires based on active fire detections outside the burned-area maps (Randerson et al., 2012). QFED v2.4 estimates global fire emissions using the MODIS measurements of fire radiative power and generates daily products at  $0.1^\circ \times 0.1^\circ$  resolution.

To drive CAM5 simulations, fire emission data were re-gridded to the model resolution and distributed vertically. For the GFED v3.1 and QFED v2.4 emission data we adopted the same injection heights (from surface to 6 km) as used in the standard CAM5 model, while for GFEDv4.1s in this study the injection heights were estimated using a fire plume model and scaled to a 6-hourly interval.

The fire emission inventories were first analyzed to select appropriate time periods and regions for our study before being used to drive model simulations. Figure 1 shows the multi-year mean biomass burning emissions from GFED v4.1 over North America. The emission manifests significant seasonality with large dry-matter consumption during March to April and June to September. The summer and autumn burning covers the Pacific Northwest and part of Canada and is mainly associated with forest fires, while the spring burning occurs in more densely populated regions like Mexico and the central and eastern United States with a large contribution of agricultural fires in croplands (Korontzi et al., 2006; Magi et al., 2012). Similar features are also captured in GFED v3.1 and QFED v2.4 with differences in the magnitude. We chose to analyze the simulated fire aerosol effect in April, the peak month of spring burning, when there are extreme fire activities over Mexico ( $10\text{--}25^\circ$  N,  $100\text{--}80^\circ$  W) and

occasionally large fires in the central US ( $35\text{--}45^\circ$  N,  $100\text{--}85^\circ$  W). For the US, an extended fire period is rare, making it necessary to perform short-term evaluation. Fire aerosols formed from these two regions are often transported to the eastern and southeastern US, where they mix with aerosols from anthropogenic sources and potentially have significant impact on clouds and radiation over these areas. Time series of regional mean fire emissions in April during 2003–2014 show that relatively large fires occurred in both regions in 2009 (Fig. S1 in the Supplement). Values of fire emissions in 2009 are larger than the multi-year April mean by a factor of 1.9 in the central US and 1.5 in southern Mexico. Thus, in the following model simulations, we focused on analyzing the aerosol properties and radiative effects over the two selected regions (denoted by the red boxes in Fig. 1) in April 2009.

Fire-emitted BC from different emission inventories in April 2009 is shown in Fig. 2. Although GFED v4.1s includes the contributions of small fires (Randerson et al., 2012), the emitted BC in GFED v4.1 shows no substantial increase compared to GFED v3.1 during the selected period. Only an increase by 1.75 is seen over southern Mexico. In the central US, the BC emission is even slightly weaker in GFED v4.1. QFED v2.4 shows a much larger BC emission than the GFED inventories. Monthly mean values of emitted BC in QFED v2.4 are larger than those in GFED v4.1s by a factor of 11.4 in the central US and a factor of 3.3 in southern Mexico.

## 2.3 Simulations

Two groups of simulations were conducted (Table 1) using the same greenhouse gas concentrations, sea surface conditions, and anthropogenic emissions of aerosols and precursors. Each group includes four simulations, performed either without fire emission or with daily fire emissions from one of the three fire emission inventories introduced in Sect. 2.2. The emitted species include BC, OC, and SO<sub>2</sub>. Horizontal winds were nudged to 6-hourly ERA-Interim reanalysis (Dee et al., 2011) as described in F. Zhang et al. (2014) in both groups.

Simulations in group A are month-long single-member nudged simulations. These simulations were performed to provide longer time series for model evaluation and generate initial condition files for simulations in group B. They started in 1 January 2009 and were integrated for 4 months with 3-month spin-up. Initial condition files were generated on 1 April at 00:00 UTC for simulations in group B.

Simulations in group B are 10-day ensemble simulations. Unlike the traditional way of perturbing initial conditions, in this study we constructed the ensembles by implementing a very weak temperature nudging and perturbing the nudging timescale. This is because under the influence of horizontal-wind nudging, ensemble differences generated by perturbing initial conditions would fade away during the integration. In

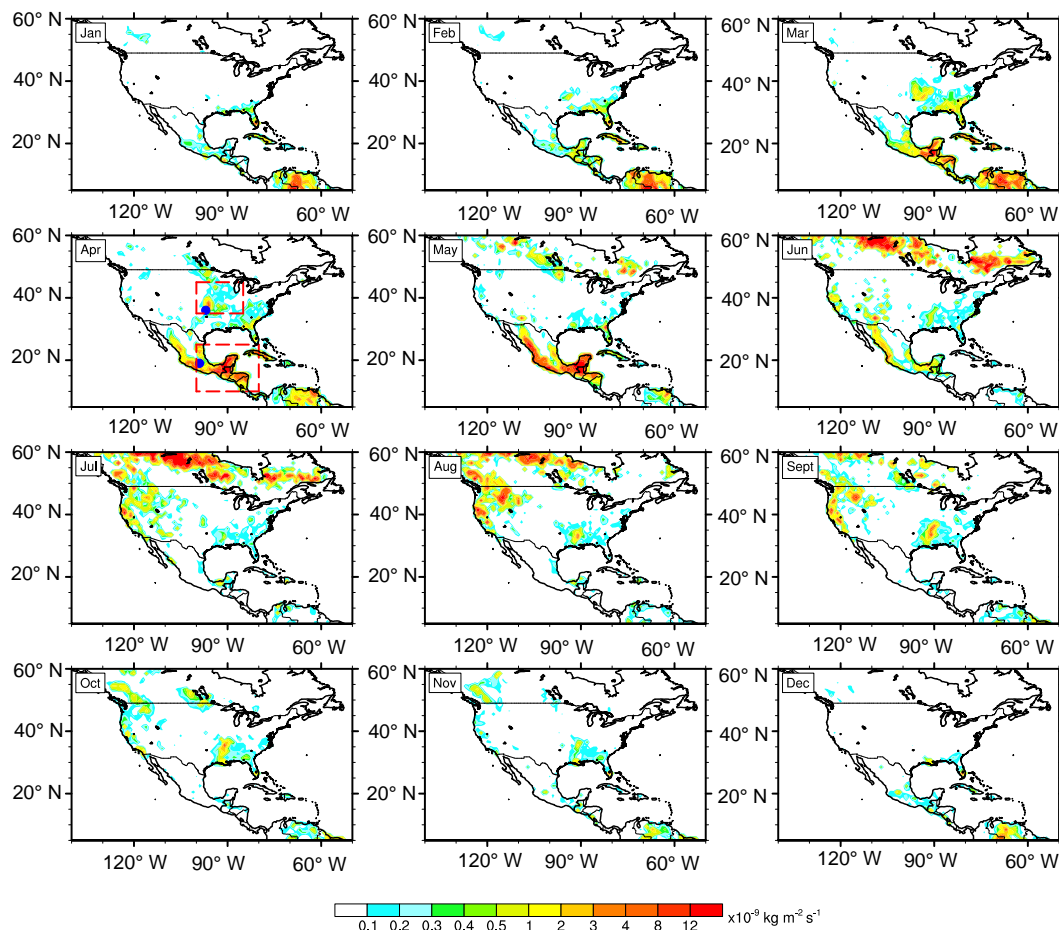


**Figure 1.** Spatial distributions of multi-year monthly mean biomass-burning-consumed dry matter over North America during 2003–2014 from GFEDv4.1. Boxes denote selected regions: central US (35–45° N, 85–100° W) and southern Mexico (10–25° N, 80–100° W). Dots denote locations of AERONET sites: CART site (36° N, 97° W) and Mexico City (19° N, 99° W).

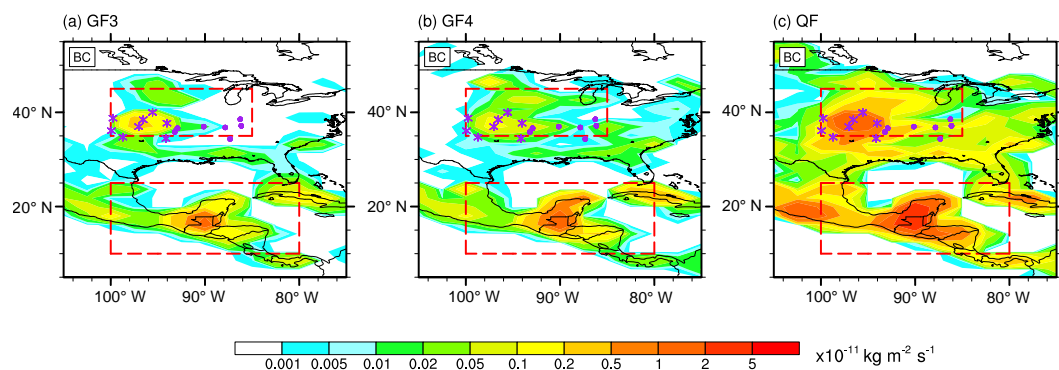


**Figure 2.** Spatial distributions of monthly mean BC emissions from three emission inventories in April 2009. IMPROVE data sites are shown as asterisks for sites near the source region and as dots for sites in the region downwind of the fire source.

contrast, our method can consider the influence of small temperature perturbations during the entire simulation period, as nudging is applied at every time step. On the other hand, the large-scale circulation patterns simulated in the different en-

semble members are very similar (not shown), so the noises caused by the chaotic system can be constrained and the effective fire aerosol forcing signal can be easily identified.

**Table 1.** List of CAM5 simulations.

Name	Fire emission	Simulation period	Member	Nudging
Group A: single-member simulations				
S_NF	No			
S_GF3	GFED v3	1 January–30 April 2009	1	Horizontal winds (6 h)
S_GF4	GFED v4.1			
S_QF	QFED v2.4			
Group B: ensemble simulations				
E_NF	No			
E_GF3	GFE D v3	1–10 April 2009	10	Horizontal winds (6 h) and temperature ( $\sim 10$ days)*
E_GF4	GFED v4.1			
E_QF	QFED v2.4			

\* See Sect. 2.3 for details about ensembles.

Each ensemble in group B includes 10 members. The only difference between the members is the relaxation timescale of temperature, which varies from 10 to 11 days at an interval of 0.1 day. All simulations started on 1 April 2009 and were integrated for 10 days. For each simulation (e.g., E\_QF), the initial condition was generated by combining the meteorological fields from initial condition outputs in the S\_NF simulation with aerosol and precursor concentrations from initial condition outputs in the single-member simulation forced by the corresponding fire emission (S\_QF).

## 2.4 Calculation of fire aerosol RF

The IPCC AR5 provides a more useful characterization of aerosol forcing by allowing for rapid tropospheric adjustments (Boucher et al., 2013) compared to the original definition of aerosol forcing. It quantifies aerosol radiative effects in terms of effective radiative forcing from aerosol–radiation interactions (ERFari) and effective radiative forcing from aerosol–cloud interactions (ERFaci). ERFari refers to the combined effect of instantaneous radiative forcing from direct scattering and absorption of sunlight (aerosol direct effect) and related subsequent rapid adjustments of atmospheric state variables and cloudiness (aerosol semi-direct effect). ERFaci refers to the indirect forcing resulting from aerosol-induced changes in cloud albedo (first albedo effect) and subsequent changes in cloud lifetime as rapid adjustments (second aerosol indirect effect) via microphysical interactions.

To allow for a straightforward comparison with previous studies in the literature, we followed the IPCC concept of including rapid adjustments (effective aerosol radiative forcing) but continued to decompose the aerosol effect in the conventional terms as aerosol DRE, aerosol cloud radiative effect (CRE) and surface albedo effect. Note that, as the nudging timescale determines the degree to which model physics are constrained (Kooperman et al., 2012), the use of a 6 h re-

laxation timescale for horizontal-wind nudging means only very fast adjustments are considered in the simulations.

Similar to Jiang et al. (2016), our calculations are based on the work of Ghan et al. (2012) and Ghan (2013). The fire aerosol DRE, CRE, and surface albedo effect are defined as fire-induced changes in aerosol forcing, cloud forcing, and surface albedo forcing, respectively, and are calculated as the difference of each item between simulations with and without fire emissions (denoted by  $\Delta$ ). In each simulation, aerosol forcing was defined as the difference between all-sky and clean-sky TOA radiative fluxes ( $F - F_{\text{clean}}$ ). Cloud forcing was defined as the difference between all-sky and clear-sky TOA radiative fluxes under clean-sky conditions ( $F_{\text{clean}} - F_{\text{clean, clear}}$ ). The rest were related to surface albedo forcing ( $F_{\text{clean, clear}}$ ). Thus fire aerosol DRE, CRE, and surface albedo effects were expressed as  $\Delta(F - F_{\text{clean}})$ ,  $\Delta(F_{\text{clean}} - F_{\text{clean, clear}})$ , and  $\Delta F_{\text{clean, clear}}$ , respectively. More details about the method can be found in Sect. 2 of Ghan (2013). CRE includes contributions of both aerosol indirect effect and aerosol semi-direct effect but was analyzed as a single term (i.e., the sum).

## 2.5 Observational data

In this study, we used two sets of AOD reanalysis and the Aerosol Robotic Network (AERONET) data (Holben et al., 1998) to evaluate the modeled AOD. The two AOD reanalysis datasets are the Naval Research Laboratory (NRL) reanalysis (Rubin et al., 2016) and the Monitoring Atmospheric Composition and Climate (MACC) reanalysis (Eskes et al., 2015). Both are generated by assimilating AOD retrievals from MODIS (Zhang et al., 2008; Benedetti et al., 2009) with forecast fields. The NRL reanalysis provides 6-hourly AOD at  $1^\circ$  horizontal resolution. The MACC dataset provides 3-hourly AOD at  $1.125^\circ$  horizontal resolution. Daily averages in April 2009 were used for model evaluation in this study. AERONET retrievals of AOD from 1 to 30 April in 2009 were used for model evaluation. Two sites

are available in the selected regions: Cloud and Radiation Testbed (Cart) site ( $36^{\circ}$  N,  $97^{\circ}$  W) and Mexico City ( $19^{\circ}$  N,  $99^{\circ}$  W). Level 2.0 cloud-screened all-points AOD at 500 and 675 nm was used to generate hourly AODs at 550 nm, which are the processed data based on a cloud-screening algorithm (Smirnov et al., 2000).

In addition, the simulated BC and primary organic matter (POM) concentrations were compared with observations from the Interagency Monitoring of Protected Visual Environments (IMPROVE) (Malm et al., 2004). IMPROVE aerosol data are only available over the central US. A total of 15 sites were selected and marked in Fig. 2, which include the sites west of  $94^{\circ}$  W near the source region (asterisks) and sites east of  $94^{\circ}$  W in the downwind region (dots). Observed organic carbon concentrations were multiplied by 1.4 for comparison with simulated POM. Detailed descriptions about the data and sites are available at <http://vista.cira.colostate.edu/improve/>. The IMPROVE network collect 24 h aerosol data on every third day. Daily averages during April 2009 are compared on IMPROVE observation days only.

### 3 Results

In this part, the model performance is first evaluated based on the simulations in group A. Next, we present the simulated short-term effective fire aerosol forcing on 10-day and daily timescales based on the results from group B simulations. We will demonstrate the importance of using ensemble simulations in estimating the short-term aerosol effective forcing and give a quantitative estimate of how many ensemble members are needed for the case selected in this study.

#### 3.1 Model evaluation

Model-simulated AODs are evaluated against the NRL and MACC reanalysis data (Fig. 3). The simulated temporal variation of regional mean AOD over the central US is consistent with that in the reanalysis, but the magnitudes of simulated AOD are lower (Fig. 3). A better agreement is found between the model and the NRL data, despite the horizontal winds in the simulation being nudged towards a reanalysis that is very similar to the data used to derive MACC. Temporal correlation coefficients (TCCs) between the modeled AOD and the NRL reanalysis are 0.87 and 0.82 for S\_QF and S\_GF4 simulations, respectively, but are lower (0.67 and 0.78) between the modeled AOD and the MACC reanalysis data. The corresponding root mean square errors (RMSEs) rise from 0.13 (S\_QF) and 0.1 (S\_GF4) to 0.23 and 0.21. Generally, AOD is underestimated by a factor of 2–4 in all simulations compared to the reanalysis, especially in simulations with GFED emissions. Previous studies have found the underestimation of AOD in simulations with GFED emissions and suggested the need to scale up GFED emissions by a factor of 1–3 to

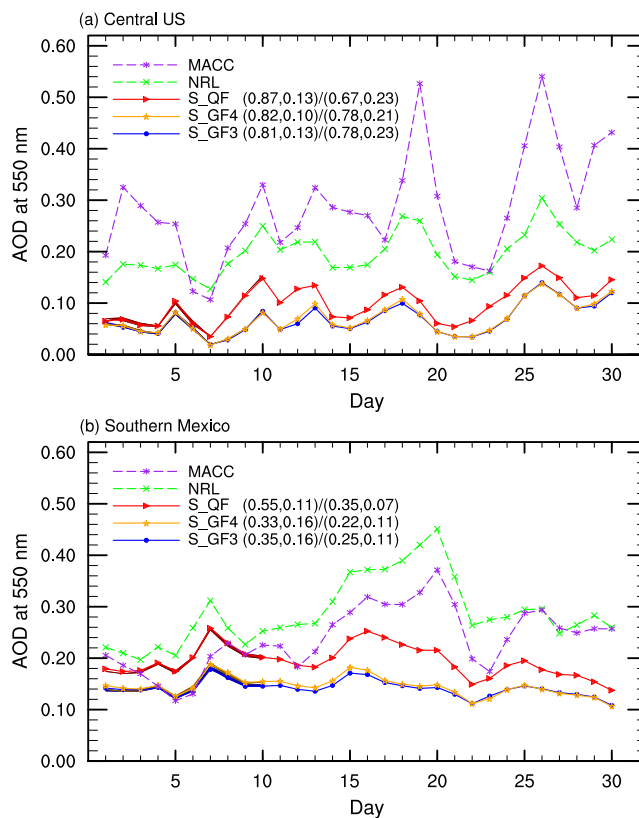


**Figure 3.** Time series of daily regional mean AOD in April 2009 in simulations and reanalysis data. Numbers in parentheses denote time correlation coefficient (TCC) and root mean square error (RMSE) between each simulation in group A and reanalysis data (left: NRL; right: MACC). Individual lines indicate group A simulations. Shaded areas (very narrow) in slightly darker colors during 1–10 April illustrate maximum and minimum values of daily mean AOD among ensemble members in group B simulations. For the single-member simulation and the ensemble simulation driven by same fire emission, the shaded area and the solid line almost overlap, given the barely indistinguishable AOD between ensemble members and the corresponding group A simulation.

match the observed AOD (Tosca et al., 2013). This is consistent with the large negative bias in the simulations S\_GF3 and S\_GF4. However, a much larger scaling factor might be needed in this case. Simulated AODs in these two simulations are almost indistinguishable due to the small difference in the total fire emission in the region.

Over Mexico, different simulations produce similar temporal variations in AOD, but the magnitude is smaller in the GFED simulations. Fire-aerosol-induced AOD increase accounts for 8.1% (S\_GF3), 11.2% (S\_GF4), and 48.8% (S\_QF) of the background AOD (Table S2 in the Supplement). Large discrepancies are found between model results and reanalysis data during 17–20 April. An increase of AOD is captured by both reanalysis datasets, while model results display a decrease of AOD compared to earlier days in the

simulation period. Note that the two sets of reanalysis data also have some differences occasionally. For example, during 10–12 April, NRL data display an increase of AOD, while MACC data show the opposite. These discrepancies may partly result from the large internal variability in this tropical region, where the simulated atmosphere state and its influence on aerosol transport are more likely to disagree between the model and the reanalysis. Generally speaking, the model forced with different fire emissions is capable of capturing daily variation of AOD in both regions, especially during 1–10 April. This period was selected for further investigation of the short-term fire aerosol effect.

Model-simulated AODs are also evaluated against AERONET retrievals (Fig. 4). At CART site ( $36^{\circ}$  N,  $97^{\circ}$  W), with the QFED emission (S\_QF) the model performs well in simulating both the temporal variation (TCC = 0.62) and magnitude of AOD. Simulations with GFED emissions also reproduce the temporal evolution well (TCC = 0.58 for S\_GF3 and 0.55 for S\_GF4), albeit with significantly low bias (mean bias by a factor of 2). The simulated difference in AOD magnitude is similar to that found by F. Zhang et al. (2014) over northern sub-Saharan African. Using the QFEDv2.4 fire emission, the simulated regional mean AOD is a factor of 1.5 higher than that using the GFEDv3.1 emission in their study. Relatively good performance of S\_QF is also seen over Mexico. The simulated time evolution agrees well with AERONET retrievals except for small discrepancies (e.g., during 17–19 April). A better agreement with the AERONET retrievals is found for the NRL data than MACC reanalysis at both sites. Consistent with the evaluation using reanalysis, the simulated temporal evolution of AOD during 1–10 April agrees well with both reanalysis data and AERONET retrievals in selected regions. This gives us further confidence in choosing this period for further investigation.

The model is further evaluated against the IMPROVE data for BC and POM mass concentrations (Fig. 5). In the downwind region, the simulated mass concentrations in the S\_QF simulation lie within a factor of 2 of the observed values at most sites. However, the magnitude is generally underestimated in simulations with the GFED emissions (S\_GF3 and S\_GF4), especially in S\_GF3. BC and POM concentrations in the downwind regions are affected by transport of aerosols from southern Mexico (Fig. S3). A larger amount of fire emission in southern Mexico would result in a higher BC (POM) concentration in the downwind region. This explains the slightly higher concentrations in the S\_GF4 simulation than in S\_GF3, as BC and POM emissions over southern Mexico are higher in GFED v4.1 due to the inclusion of small fires (Randerson et al., 2012). The good agreement between S\_QF and observations suggests that the QFED data have a reasonable total emission rate. However, in the source region, the S\_QF simulation displays a large positive bias with a large majority of the values falling out of the a-factor-of-2 band. Given the reasonable total emission rate in QFED

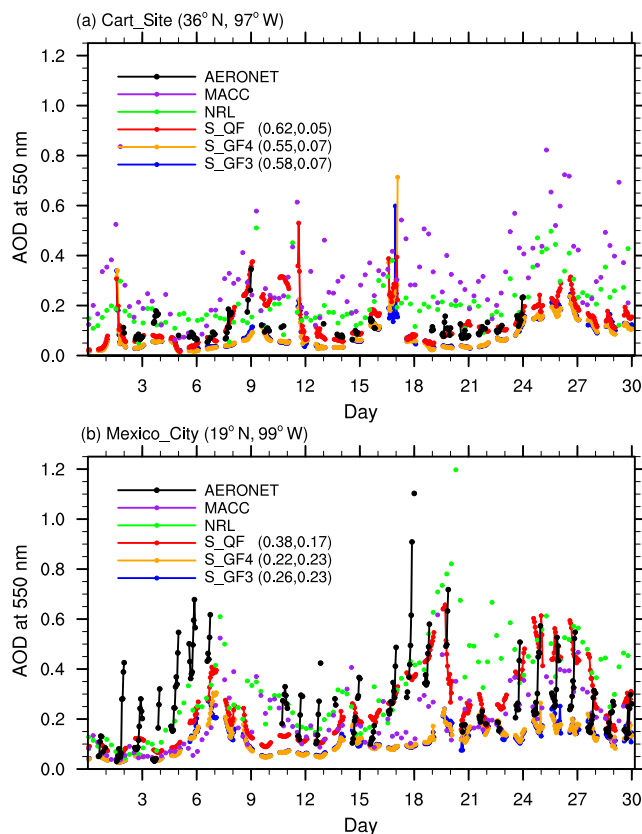


**Figure 4.** Time series of hourly regional mean AOD in April 2009 from group A simulations, reanalysis data and AERONET retrievals at AERONET sites. Numbers in parentheses denote TCC (left) and RMSE (right) between each simulation and AERONET AOD.

and a good agreement of AOD with AERONET retrievals at CART site, this might result from the discrepancies in the vertical distribution of the fire emissions. Fire-emitted BC and POM in simulations S\_QF and S\_GF3 reach maximum values in the lowest level and decrease sharply to the next level, while low-level fire emissions in S\_GF4 are distributed in a more uniform way (Fig. S4). The fact that the sampling was done on the lowest model level at most sites to compare with the IMPROVE data explains the strong overestimation in S\_QF. Although the same impact from vertical distribution of the fire emission also appears in the S\_GF3 simulation, it is partly offset by its negative bias in the total emission rate.

### 3.2 10-day-mean results

Given the good model performance during 1–10 April, we proceed to analyze the short-term effects of fire aerosols during this period with nudged ensemble simulations. We define “fire AOD” as the AOD difference between the simulations with and without fire emissions.

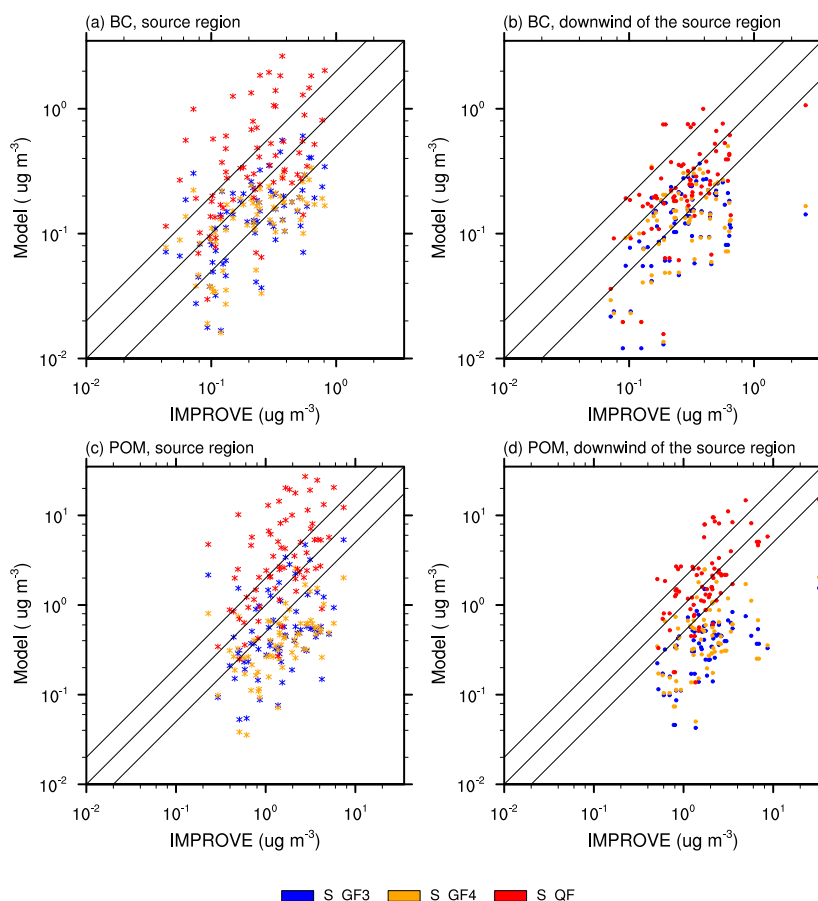


**Figure 5.** Evaluation of simulated BC (a, b) and POM (c, d) concentrations in group A simulations against the IMPROVE data at sites near the source and downwind of the source region. Locations of these sites are marked with the same symbol in Fig. 2.

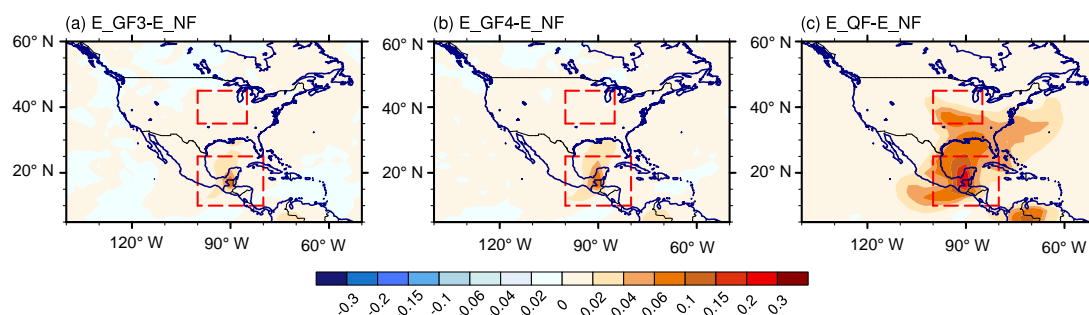


**Figure 6.** Spatial distributions of 10-day-average (1–10 April) ensemble mean AOD differences between simulations with (E\_GF3, E\_GF4, and E\_QF) and without (E\_NF) fire emission.

### 3.2.1 Fire aerosol distribution

Figure 6 shows the spatial distributions of 10-day-average ensemble mean fire AOD. For reference, the total AOD in the simulation without fire emissions is shown in Fig. S2. During the period, regional mean AOD increases by 6.4 % (E\_GF3), 6.4 % (E\_GF4), and 70.2 % (E\_QF) in the central US and 10.4 % (E\_GF3), 13.3 % (E\_GF4), and 49.6 % (E\_QF) in

southern Mexico when fire emissions are included. In E\_QF, high fire AOD covers almost the entire selected region and extends further north. Maximum values of fire AOD stay above 0.2 around the Yucatán Peninsula. Over the central US, significant fire AOD ranging between 0.04 and 0.1 appears in the southwest part of the selected region. Apart from the significant AOD difference in selected regions, large fire AOD also appears near the eastern coast as a result of local

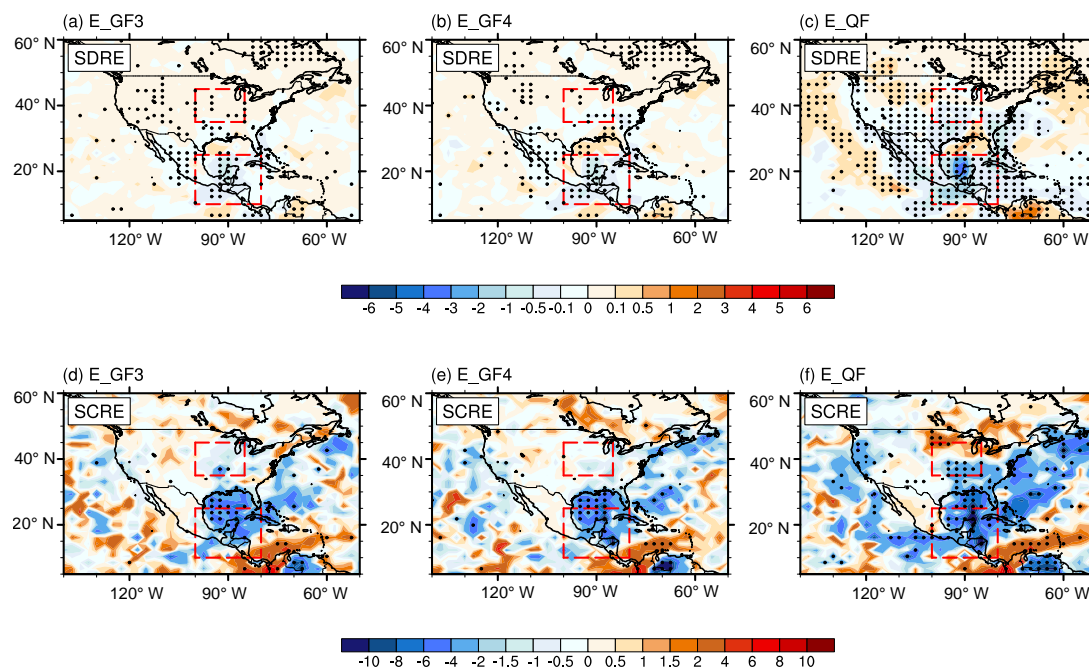


**Figure 7.** Spatial distributions of 10-day-average (1–10 April) ensemble mean fire aerosol shortwave direct radiative effect (SDRE) and shortwave cloud radiative effect (SCRE) ( $\text{W m}^{-2}$ ) in group B simulations. Dots denote regions where SDRE is statistically significant at the 95 % confidence level based on the Kolmogorov–Smirnov (KS) test.

fire emission and the eastward transport of fire aerosols from both regions. Overall, the modeled fire AOD is much smaller in simulations with GFED emissions.

### 3.2.2 Fire aerosol radiative effect

As described in Sect. 2.4, the fire aerosol radiative effect can be decomposed into three items: fire aerosol DRE, fire aerosol CRE, and fire aerosol surface albedo effect (Table S3). Figure 7 shows the spatial distributions of the shortwave direct radiative effect (SDRE) and shortwave cloud radiative effect (SCRE). They are major contributors to the total fire aerosol forcing in the selected regions. For reference, total aerosol forcing and total shortwave cloud forcing in the simulation without fire emissions are shown in Fig. S2. The spatial distribution of SDRE and SCRE are similar for the three cases but have different magnitudes and statistical significant regions for simulations with QFED and GFED fire emissions. In the central US, fire aerosol SDRE is negligible in GFED-forced simulations due to small fire AOD. Although the fire AOD is larger in the E\_QF simulation, the compensation between the warming effect of fire BC and the cooling effect of fire POM still results in a weak forcing of about  $-0.1 \text{ W m}^{-2}$ . Over southern Mexico, all simulations produce significant cooling by fire aerosol SCRE with maximum values 3 times as large as those of corresponding SDRE. For both SDRE and SCRE, the largest fire aerosol effects appear in the E\_QF simulation, while the E\_GF3 yields

the weakest forcing, which is consistent with the modeled fire AOD in these simulations.

In the following analysis, we will focus on the results from the E\_QF simulation. Both SDRE and SCRE spread outside the two selected regions and extend eastward, reaching coastal regions. A stronger fire aerosol effect is seen in the southern Mexico region. Strong SDRE appears over the Yucatán Peninsula, where fire AOD peaks (Fig. 6). Regional mean 10-day averages of SDRE and SCRE reach  $-0.86$  and  $-3.0 \text{ W m}^{-2}$ , respectively. It is interesting to note that the maximum SCRE tends to center around the adjacent Gulf of Mexico rather than the land region. In the central US, a positive SCRE exceeding  $2 \text{ W m}^{-2}$  appears in the northern part of the region, while a comparable negative SCRE appears in the southern part of the region.

To find out the causes of the fire aerosol SCRE, fire-aerosol-induced changes in cloud properties are analyzed. Given the largely insignificant change in cloud fraction (Fig. 8), the negative fire aerosol SCRE in both regions is mainly associated with increases in liquid water path (LWP) and droplet number concentration (CDNC). The increased CDNC due to an increase of cloud condensation nuclei (CCN) from fire aerosols (Fig. 8) leads to smaller droplet sizes, which in turn increase cloud albedo by enhancing backscattering (Twomey, 1977) and further affect LWP by decreasing precipitation efficiency and allowing more liquid water to accumulate (Albrecht, 1989; Ghan et al., 2012). These changes in warm-cloud properties demonstrate impor-

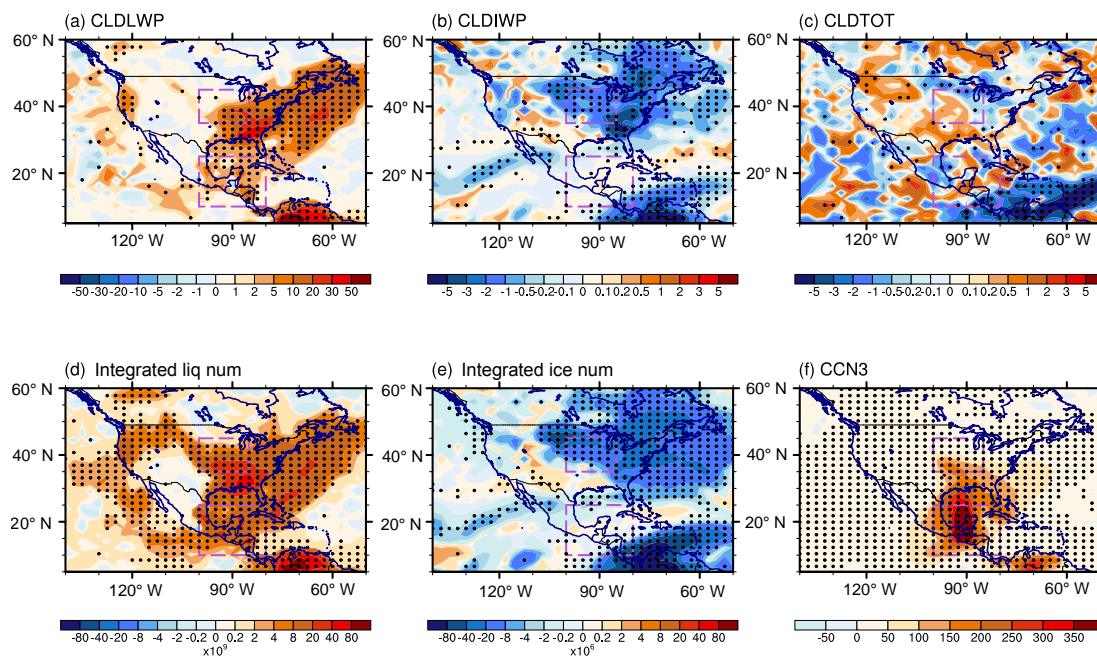


**Figure 8.** Difference of 10-day-average (1–10 April) ensemble mean between simulations E\_NF and E\_QF: (a) cloud liquid water path ( $\text{g m}^{-2}$ ), (b) cloud ice water path ( $\text{g m}^{-2}$ ), (c) total cloud fraction (%), (d) column-integrated droplet number concentration ( $\text{m}^{-2}$ ), (e) column-integrated ice number concentration ( $\text{m}^{-2}$ ), and (f) cloud condensation nuclei at 0.1 % supersaturation near 900 hPa. Dots denote regions where the difference is statistically significant at the 95 % confidence level based on the KS test.

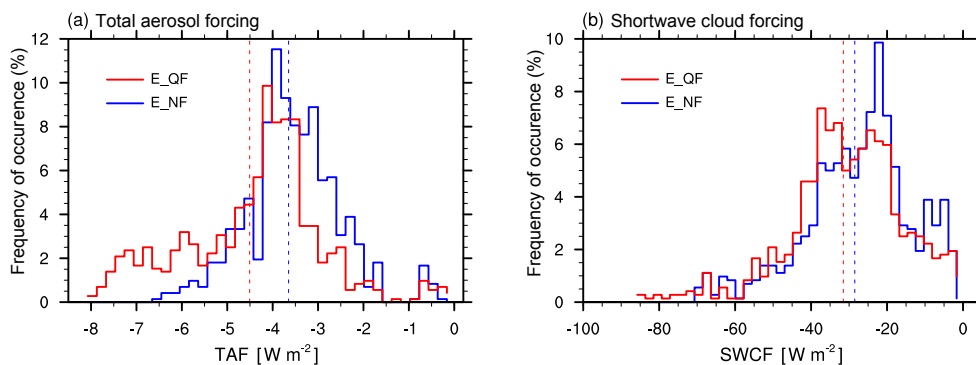


**Figure 9.** Probability distributions of 10-day-average (1–10 April) (a) total aerosol forcing and (b) total shortwave cloud forcing over southern Mexico in simulations E\_NF and E\_QF sampled from grid values of ensemble members ( $72 \times 10$  for each case). Dashed lines indicate the mean of the distribution.

tant contributions of both aerosol first and second indirect effects to the negative SCRE. Over southern Mexico, although changes of CDNC and LWP are of comparable magnitudes between the Gulf of Mexico and the land region (Fig. 8), relative changes of both quantities are much larger over the Gulf of Mexico (Fig. S5) due to the smaller magnitudes of background CDNC and LWP over the region (Fig. S6), which tend to lead to a more sensitive response of SCRE. That is why the maximum SCRE over southern Mexico is centered over the Gulf of Mexico. Changes in ice water path (IWP) and ice crystal number concentration (ICNC) can also significantly affect SCRE, albeit with an opposite sign and mostly

in the central US. The decreased IWP and ICNC, which are possibly caused by fire-aerosol-induced changes in the circulation (Ten Hoeve et al., 2012) and reduced coarse-mode dust aerosol concentrations (Fig. S7), are responsible for the positive SCRE and the negative longwave cloud radiative effect (Table S3) in the northern part of the central US. In the southern part of the central US, the reduction of IWP and ICNC also results in a positive SCRE, which partly offsets the negative SCRE resulting from changes in warm-cloud properties. This explains the weaker total negative SCRE in this region than in the southern Mexico region despite the more substantial increase in CDNC and LWP here. In the northeast of the

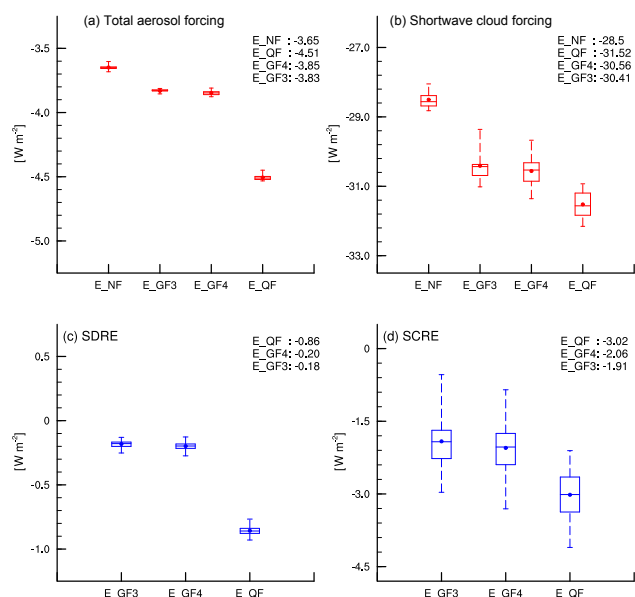


**Figure 10.** 10-day-average (1–10 April) regional mean (a) total aerosol direct forcing, (b) total shortwave cloud forcing, (c) SDRE, and (d) SCRE in southern Mexico in group B simulations. Boxes denote the 25th and 75th percentiles. Bars outside the box indicate minimum and maximum. Bar within the box denotes the 50th percentile. Total aerosol and cloud forcing are sampled from different ensemble members (10 for each case). Fire aerosol SDRE and SCRE are sampled by calculating the difference between members in simulations E\_QF (E\_GF3/E\_GF4) and E\_NF (10 × 10 for each case).

extended coastal regions, a more significant change of LWP comparable to that in the central US appears, while a more significant change of CDNC comparable to that in southern Mexico occurs in the southwest. The combined effect leads to the total fire aerosol effect in the extended regions.

The ensemble method provides another effective way to distinguish the fire aerosol radiative effect by comparing the radiative forcing distribution of ensemble members between simulations with and without fire emission. A significant difference in the distribution of total aerosol (cloud) forcing indicates a significant fire aerosol direct (cloud) effect. As shown in Fig. 9, a shift towards stronger magnitude occurs to the total aerosol forcing when fire aerosols are considered. The E\_QF simulation has a larger percentage of grid cells with SDRE below  $-4.2 \text{ W m}^{-2}$ , while more grid cells exceed  $-4.2 \text{ W m}^{-2}$  in E\_NF, which indicates a significant negative fire aerosol direct effect. The same shift also appears in the total shortwave cloud forcing, with more grid cells having shortwave cloud forcing below  $-30 \text{ W m}^{-2}$  in the E\_QF simulation. Regional mean total aerosol and shortwave cloud forcing in southern Mexico become more negative ( $-0.86$  and  $-3.0 \text{ W m}^{-2}$ ) with fire aerosols.

Figure 10 illustrates ensemble behavior of 10-day-average regional mean total aerosol and cloud forcing from all sim-

ulations as well as resulted fire aerosol SDRE and SCRE. The GFED-forced simulations not only resemble in ensemble mean but also have small differences in ensemble member distribution. Although members in the E\_QF simulation capture stronger aerosol forcing, and thus stronger fire aerosol SDRE than those in E\_GF3 and E\_GF4, the ensemble spread (as indicated by the maximum and minimum values) in the three simulations is similar. Moreover, the E\_QF simulation yields a smaller spread of SCRE than the GFED-forced simulations despite a stronger ensemble mean SCRE. In each fire simulation, ensemble mean fire aerosol SCRE has a much larger magnitude than SDRE, as does the corresponding ensemble spread. Taking results from the E\_QF simulation as an example, the ensemble spread of SCRE reaches  $0.47 \text{ W m}^{-2}$ , accounting for 15.6 % of the corresponding ensemble mean, while the ensemble spread of SDRE is  $0.03 \text{ W m}^{-2}$ , accounting for 3.5 % of the corresponding ensemble mean.

### 3.3 Daily RF

The fire aerosol effect is also investigated for individual days. The spatial distributions of SDRE and SCRE on 7 April are shown in Fig. 11, when relatively high fire emissions appear in both regions. Negative fire aerosol SDRE appears in the central US biomass burning region, indicating the dominant role of POM scattering. Fire aerosol SDRE over southern Mexico shows the contrast of a warming effect in land region and a cooling effect in the adjacent ocean despite similar aerosol loading in the two regions. However, they do have nearly equal clear-sky BC absorption and POM scattering (Fig. 12). Difference in low-level cloud distributions between the two regions leads to different signs of the simulated all-sky SDRE. Over land, when clouds appear under elevated aerosol layers, more solar radiation is reflected back to space, and this leads to amplified BC absorption and more positive direct aerosol forcing (Keil and Haywood, 2003; Zhang et al., 2016; Jiang et al., 2016). In contrast, neither absorption nor scattering changes significantly from clear-sky to all-sky conditions over adjacent areas over the ocean, since the small cloud fraction is small. The same enhanced absorption of above-cloud aerosols is also found over the west Atlantic Ocean. Fire aerosols produce remarkably negative SCRE up to  $-16 \text{ W m}^{-2}$  over southern Mexico land in response to the increase in CDNC and LWP.

### 3.4 Discussion about simulation strategy

Figure 13 shows the daily variation of the regional mean total (direct) aerosol forcing and cloud forcing. Both the ensemble mean and spread are investigated here. The total aerosol and cloud forcing exhibit considerable diversity across ensemble members within each simulation even though the simulated AOD is nearly indistinguishable (Fig. 3). Taking results from the E\_QF simulation as an example, maximum values of

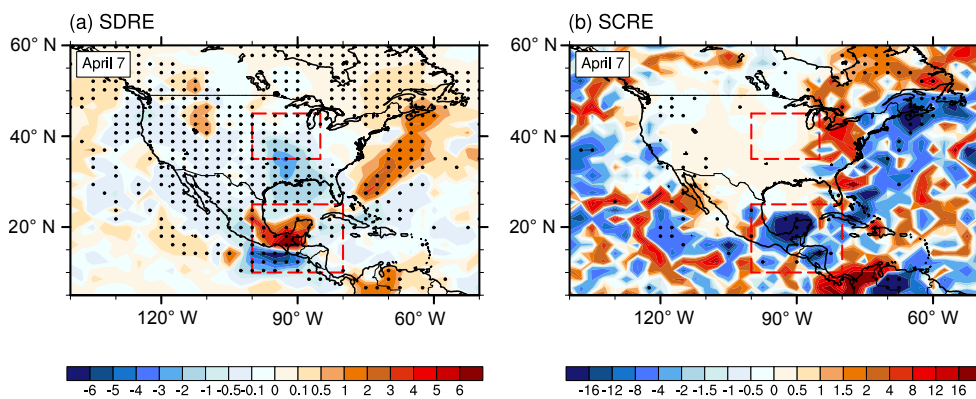


**Figure 11.** Spatial distributions of ensemble mean fire aerosol (a) SDRE and (b) SCRE ( $\text{W m}^{-2}$ ) on 7 April in the E\_QF simulation. Dots denote grids where the fire aerosol effect is statistically significant at the 95 % confidence level based on the KS test.

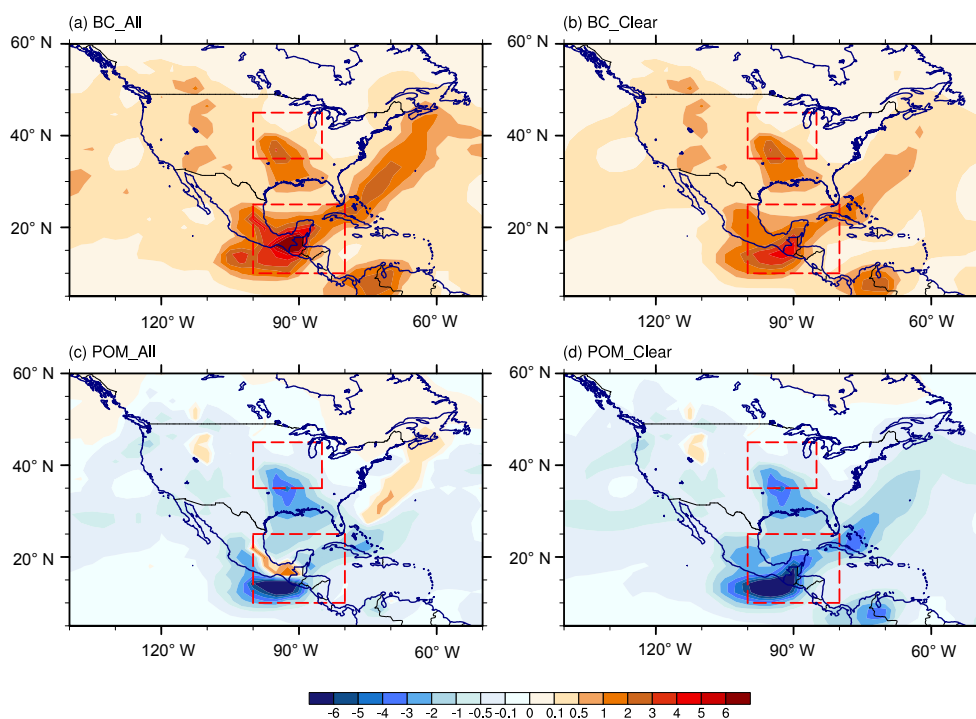


**Figure 12.** Spatial distributions of fire BC SDRE and fire POM SDRE ( $\text{W m}^{-2}$ ) under all-sky and clear-sky conditions on 7 April in the E\_QF simulation.

difference between members exceed  $0.4 \text{ W m}^{-2}$  for aerosol forcing and  $5 \text{ W m}^{-2}$  for cloud forcing, which are approximately 10 % of the corresponding ensemble mean values. The large spread of total aerosol forcing and cloud forcing will lead to uncertainties in the estimation of fire aerosol effect. This points out the importance of conducting ensemble simulations in order to get a more comprehensive estimate of the daily fire aerosol effect. The minimum ensemble size required for this case is investigated in terms of the ensemble mean and spread estimate. Simulated ensemble mean fire aerosol SDRE remains nearly unchanged regardless of

the ensemble size (Fig. 14a). However, discrepancies in the ensemble mean fire aerosol SCRE (Fig. 14b) are substantial when the number of ensemble members is small. The same is true for the ensemble spread of fire aerosol SCRE (Fig. S8). In order to quantify the discrepancies of the simulated SCRE, we chose the ensemble mean SCRE in the 20-member simulation as a reference and use the RMSE of the ensemble mean SCRE in the  $N$ -member simulation to quantify the deviation of the simulated SCRE from the reference value. It is calculated as the standard deviation of the differences between the daily ensemble mean SCRE in the  $N$ -member simulation

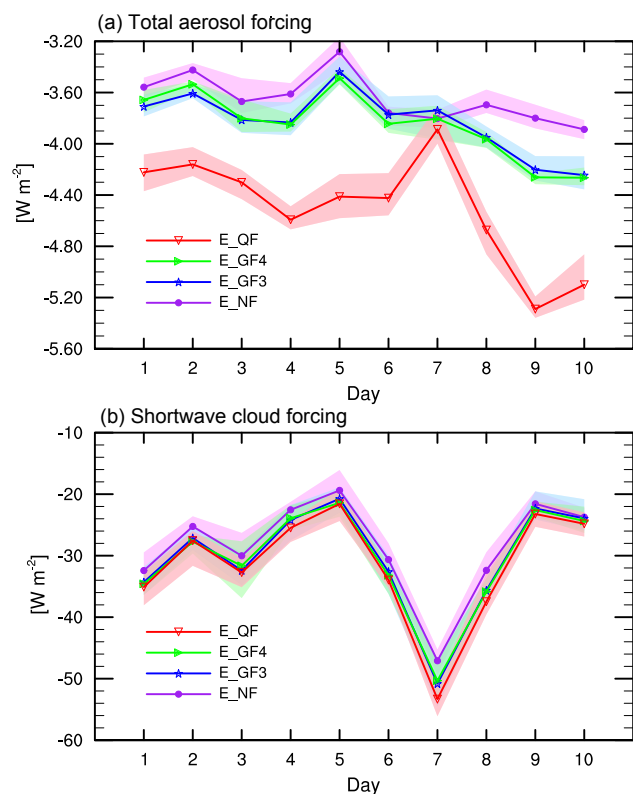


**Figure 13.** Time series of daily regional mean total (a) aerosol forcing and (b) cloud forcing in southern Mexico during 1–10 April 2009 in group B simulations. Individual lines indicate ensemble mean values. Shaded areas illustrate the ensemble spread (from minimum to maximum).

and the 20-member simulation. For each  $N$ , we randomly sampled 1000 times from the 20 members to help reduce the influence from limited sampling. Figure 15 shows that both the RMSE of ensemble mean SCRE and the difference of RMSE between the 1000 groups of simulations (for each  $N$ ) decrease with increasing  $N$ . The minimum number of  $N$  required is determined when the 90th percentile of RMSE is smaller than a threshold RMSE. Without a good reference, we set the threshold RMSE to 20 % ( $0.566 \text{ W m}^{-2}$ ) of the reference 10-day-mean SCRE ( $-2.83 \text{ W m}^{-2}$ ). As shown in Fig. 15, at least 11 members are needed to meet this criterion.

Fire aerosol sources are often intermittent and height-dependent, and there is a need to estimate the short-term effective aerosol forcing. Although nudging helps to constrain large-scale features, the simulated cloud properties (e.g., cloud fraction and LWP) and their response to aerosol changes can still be sensitive to small perturbations in the atmospheric state. Therefore, for investigating the short-term aerosol effect, a single simulation might not be sufficient to tell whether the aerosol effect is significant. The use of ensembles provides an effective way to estimate the uncertainty. Previous investigations of the short-term fire aerosol

effect are mainly based on single-member simulations (Wu et al., 2011; Sena et al., 2013; Kolusu et al., 2015). While this might be less a problem for SDRE, one should be more careful when investigating the aerosol indirect effect and conduct ensemble simulations to see whether the estimated fire aerosol effects are robust.

## 4 Summary

In this study, we investigated the short-term effect of fire aerosols on cloud and radiation using CAM5 simulations. Month-long single-member simulations and 10-day ensemble simulations were conducted in April 2009. In order to help extract signals on short timescales, we used nudging to constrain horizontal winds in all simulations. Our investigation focused on southern Mexico, where there were constant intensive fire activities, and the central US, with occasionally large fires. Apart from the local effect, fire emissions from the two regions are shown to affect downwind coastal regions through transport.

Modeled AOD and mass concentrations (BC and POM) were evaluated against observations. In general, all simulations with fire emissions reproduce the observed temporal variation of daily mean AOD well, although the simulated magnitude is smaller. The model performance is better when QFEDv2.4 is used, which has larger fire emissions. Modeled regional mean AOD values in simulations using two versions of GFED fire emission data are barely distinguishable, despite the inclusion of small fires and changed injection heights in GFEDv4.1 used in this study. Both simulate about a factor-of-1.5-smaller AOD than that in the simulation using the QFED fire emissions. At sites in the downwind region, the modeled BC and POM mass concentrations in the simulation with QFEDv2.4 emission (S\_QF) agree well with the IMPROVE data. In contrast, simulations with the other two fire emission datasets (S\_GF3 and S\_GF4) have a low bias. The simulated AOD in the source region in S\_QF also agrees well with the AERONET data (CART site). If there is no large compensating error in the model, QFEDv2.4 seems more reasonable in terms of the total (vertically integrated) emission rate. On the other hand, S\_QF strongly overestimates BC and POM concentrations in the source region. Considering that the source-region AOD and the downwind surface mass concentrations are well simulated, the overestimation suggests the actual emission peak might appear at higher levels than the height-dependent injection rates applied in the S\_QF simulation.

Based on the evaluation, we chose the first 10 days as the simulation period and focused on the simulation with QFEDv2.4 fire emission in our nudged-ensemble simulations. In our method, the nudged ensembles are generated by adding a very weak temperature nudging along with horizontal-wind nudging and perturbing the nudging timescale of temperature gently. In this way, small temper-

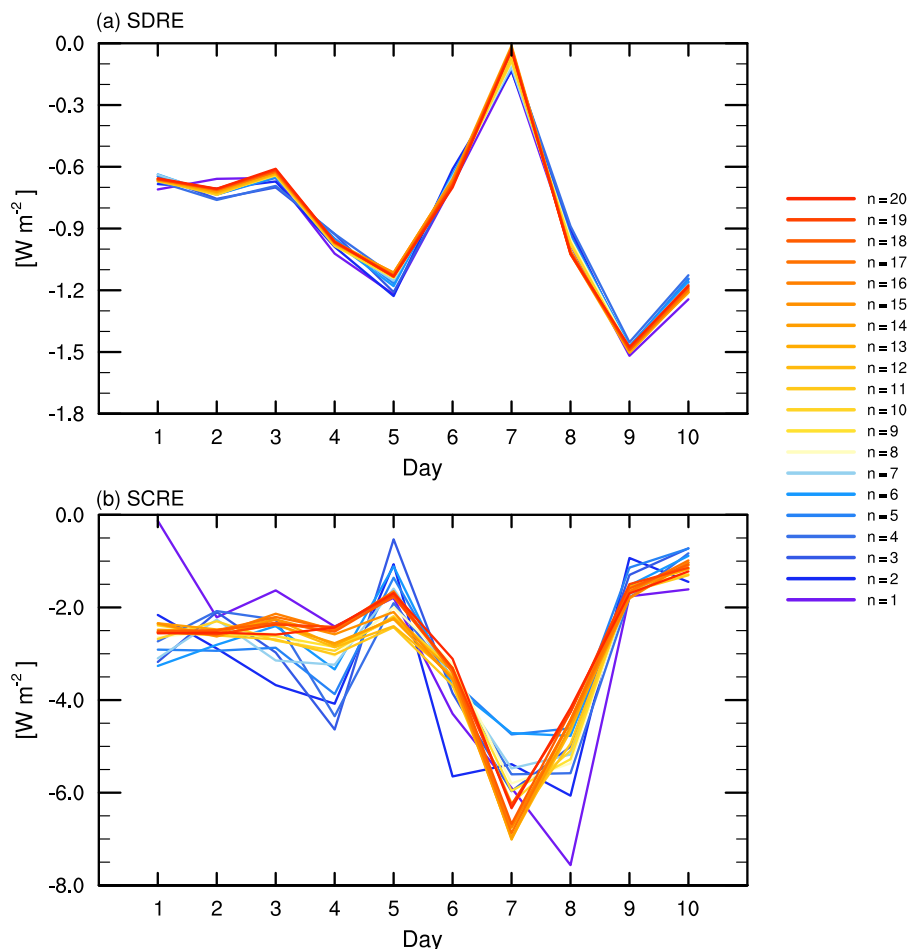


**Figure 14.** Time series of daily ensemble mean fire aerosol (a) SDRE and (b) SCRE averaged over southern Mexico during 1–10 April 2009 in QFED-forced ensemble simulations with varying total ensemble member numbers ( $n = 1–20$ ).

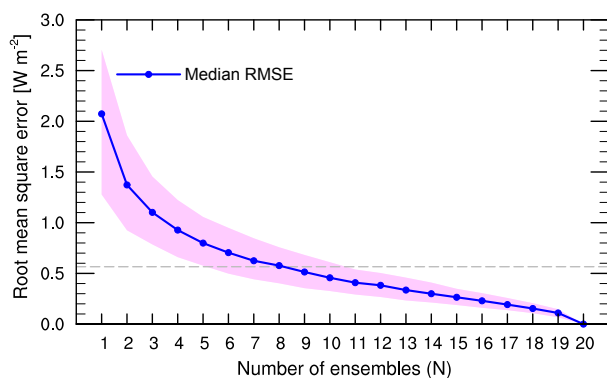


**Figure 15.** Root mean square error (RMSE) of the ensemble mean of the regional mean fire aerosol SCRE during 1–10 April over southern Mexico in simulations with different total numbers of ensemble members ( $N$ ). The blue line represents the median RMSE of the 1000 groups (each group has  $N$  members/simulations). The grey line represents the threshold RMSE. Shaded area denotes the range between the 10th and 90th percentiles.

ature perturbations are added to the simulation at each time step, while the large-scale circulation features are very similar between individual members. We first investigated the 10-day-mean effective fire aerosol forcing. Decomposition of total aerosol radiative forcing shows that fire aerosol effects in the two selected regions are dominated by the SCRE. All fire simulations show similar spatial distribution of SDRE and SCRE, albeit with different magnitudes and statistically significant regions. The similarity in the spatial distribution is expected since the three emission datasets differ mainly in the emission magnitude and not much in spatial distribution in the focus regions of this study. Fire aerosol effects in simulations with GFED emissions ( $E_{GF3}$  and  $E_{GF4}$ ) are weaker than with QFEDv2.4 emissions ( $E_{QF}$ ) by a factor of 1.5 for SCRE and a factor of more than 4 for SDRE. Overall, the difference in simulated AOD and fire aerosol indirect radiative effects between simulations is smaller than the difference between fire emissions, consistent with the findings in the sub-Saharan African biomass burning region (F. Zhang et al., 2014).

Fire aerosols produce a negative direct effect of  $-0.1 \text{ W m}^{-2}$  in the central US and  $-0.86 \text{ W m}^{-2}$  in southern Mexico in E\_QF during the 10-day period. Within each region, negative fire aerosol SDRE peaks where fire AOD reaches its maximum. Unlike the limited area affected by significant fire aerosol SDRE, fire aerosol SCRE from selected regions spreads eastward and northward, affecting remote coastal regions. Ensemble mean results show strong SCRE over almost the entirety of southern Mexico, with a 10-day regional mean value of  $-3.0 \text{ W m}^{-2}$ . Over the central US, the SCRE is positive in the north and negative in the south, and the regional mean is small ( $-0.56 \text{ W m}^{-2}$ ). Maximum SCRE stays below  $-4 \text{ W m}^{-2}$  in the (southern) central US and  $-10 \text{ W m}^{-2}$  in southern Mexico in response to significantly increased LWP and CDNC. Decreases of IWP and ICNC also contribute to fire aerosol SCRE in the central US but with an opposite sign. The offset effect of the positive forcing induced by changes in cloud ice properties explains the smaller SCRE in the central US despite the larger changes in cloud droplet properties.

We also investigated fire aerosol effects on a daily timescale, where the variation in the simulated fire aerosol effect can be large among the ensemble members. The large ensemble spread of total aerosol and cloud forcing indicates large uncertainties in estimating daily fire aerosol effects, despite similar AOD across ensemble members. Further investigations show that the simulated ensemble mean and spread with fewer than seven members differs considerably from those with more members. Our results suggest that, for short-term simulations of aerosol and cloud processes, even small perturbations might result in large difference across members despite constrained large-scale features. In order to obtain a robust estimate of the effective fire aerosol forcing during a short period, it is important to conduct ensemble simulations with sufficient ensemble members.

*Data availability.* All model results are available from the corresponding author upon request.

**The Supplement related to this article is available online at <https://doi.org/10.5194/acp-18-31-2018-supplement>.**

*Competing interests.* The authors declare that they have no conflict of interest.

*Acknowledgements.* We thank two anonymous reviewers for their careful reviews and suggestions that helped to greatly improve the analyses and discussion presented in this paper. This study was supported by the US Department of Energy (DOE)'s Office of Science as part of the Regional and Global Climate Modeling Program

(NSF-DOE-USDA EaSM2). The work was also supported by the National Natural Science Foundation of China (NSFC) under grant nos. 41621005 and 41330420, the National Key Basic Research Program (973 Program) of China under grant no. 2010CB428504, and the Jiangsu Collaborative Innovation Center of Climate. The Pacific Northwest National Laboratory (PNNL) is operated for DOE by Battelle Memorial Institute under contract DE-AC05-76RL01830. Computations were performed using resources of the National Energy Research Scientific Computing Center (NERSC) at Lawrence Berkeley National Laboratory and PNNL Institutional computing.

Edited by: Yves Balkanski

Reviewed by: two anonymous referees

## References

- Albrecht, B. A.: Aerosols, cloud microphysics, and fractional cloudiness, *Science*, 245, 1227–1231, 1989.
- Benedetti, A., Morcrette, J. J., Boucher, O., Dethof, A., Engelen, R., Fisher, M., Flentje, H., Huneeus, N., Jones, L., and Kaiser, J.: Aerosol analysis and forecast in the European centre for medium-range weather forecasts integrated forecast system: 2. Data assimilation, *J. Geophys. Res.*, 114, D13205, <https://doi.org/10.1029/2008JD011115>, 2009.
- Bond, T. C., Doherty, S. J., Fahey, D., Forster, P., Berntsen, T., DeAngelo, B., Flanner, M., Ghan, S., Kärcher, B., and Koch, D.: Bounding the role of black carbon in the climate system: A scientific assessment, *J. Geophys. Res.-Atmos.*, 118, 5380–5552, 2013.
- Bony, S., Colman, R., Kattsov, V. M., Allan, R. P., Bretherton, C. S., Dufresne, J.-L., Hall, A., Hallegatte, S., Holland, M. M., and Ingram, W.: How well do we understand and evaluate climate change feedback processes?, *J. Climate*, 19, 3445–3482, 2006.
- Boucher, O., Randall, D., Artaxo, P., Bretherton, C., Feingold, G., Forster, P., Kerminen, V.-M., Kondo, Y., Liao, H., and Lohmann, U.: Clouds and aerosols, in: *Climate change 2013: the physical science basis. Contribution of Working Group I to the Fifth Assessment Report of the Intergovernmental Panel on Climate Change*, Cambridge University Press, 571–657, 2013.
- Brito, J., Rizzo, L. V., Morgan, W. T., Coe, H., Johnson, B., Haywood, J., Longo, K., Freitas, S., Andreae, M. O., and Artaxo, P.: Ground-based aerosol characterization during the South American Biomass Burning Analysis (SAMBBA) field experiment, *Atmos. Chem. Phys.*, 14, 12069–12083, <https://doi.org/10.5194/acp-14-12069-2014>, 2014.
- Chen, D., Liu, Z., Schwartz, C. S., Lin, H.-C., Cetola, J. D., Gu, Y., and Xue, L.: The impact of aerosol optical depth assimilation on aerosol forecasts and radiative effects during a wild fire event over the United States, *Geosci. Model Dev.*, 7, 2709–2715, <https://doi.org/10.5194/gmd-7-2709-2014>, 2014.
- Chubarova, N., Nezval', Ye., Sviridenkov, I., Smirnov, A., and Slutsker, I.: Smoke aerosol and its radiative effects during extreme fire event over Central Russia in summer 2010, *Atmos. Meas. Tech.*, 5, 557–568, <https://doi.org/10.5194/amt-5-557-2012>, 2012.
- Chubarova, N. Y., Prilepsky, N. G., Rublev, A. N., and Riebau, A. R.: A Mega-Fire event in central Russia: fire weather, radiative,

- and optical properties of the atmosphere, and consequences for subboreal forest plants, *Dev. Environm. Sci.*, 8, 247–264, 2008.
- Dee, D., Uppala, S., Simmons, A., Berrisford, P., Poli, P., Kobayashi, S., Andrae, U., Balmaseda, M., Balsamo, G., and Bauer, P.: The ERA-Interim reanalysis: Configuration and performance of the data assimilation system, *Q. J. Roy. Meteor. Soc.*, 137, 553–597, 2011.
- Eskes, H., Huijnen, V., Arola, A., Benedictow, A., Blechschmidt, A.-M., Botek, E., Boucher, O., Bouarar, I., Chabrilat, S., Cuevas, E., Engelen, R., Flentje, H., Gaudel, A., Griesfeller, J., Jones, L., Kapsomenakis, J., Katragkou, E., Kinne, S., Langerock, B., Razinger, M., Richter, A., Schultz, M., Schulz, M., Sudarchikova, N., Thouret, V., Vrekoussis, M., Wagner, A., and Zerefos, C.: Validation of reactive gases and aerosols in the MACC global analysis and forecast system, *Geosci. Model Dev.*, 8, 3523–3543, <https://doi.org/10.5194/gmd-8-3523-2015>, 2015.
- Ghan, S. J., Liu, X., Easter, R. C., Zaveri, R., Rasch, P. J., Yoon, J.-H., and Eaton, B.: Toward a minimal representation of aerosols in climate models: Comparative decomposition of aerosol direct, semidirect, and indirect radiative forcing, *J. Climate*, 25, 6461–6476, 2012.
- Ghan, S. J.: Technical Note: Estimating aerosol effects on cloud radiative forcing, *Atmos. Chem. Phys.*, 13, 9971–9974, <https://doi.org/10.5194/acp-13-9971-2013>, 2013.
- Giglio, L., Randerson, J. T., and van der Werf, G. R.: Analysis of daily, monthly, and annual burned area using the fourth-generation global fire emissions database (GFED4), *J. Geophys. Res.-Biogeo.*, 118, 317–328, <https://doi.org/10.1002/jgrg.20042>, 2013.
- Holben, B. N., Eck, T., Slutsker, I., Tanre, D., Buis, J., Setzer, A., Vermote, E., Reagan, J., Kaufman, Y., and Nakajima, T.: AERONET – A federated instrument network and data archive for aerosol characterization, *Remote Sens. Environ.*, 66, 1–16, 1998.
- Iacono, M. J., Delamere, J. S., Mlawer, E. J., Shephard, M. W., Clough, S. A., and Collins, W. D.: Radiative forcing by long-lived greenhouse gases: Calculations with the AER radiative transfer models, *J. Geophys. Res.*, 113, D13103, <https://doi.org/10.1029/2008JD009944>, 2008.
- Jacobson, M. Z.: Effects of biomass burning on climate, accounting for heat and moisture fluxes, black and brown carbon, and cloud absorption effects, *J. Geophys. Res.-Atmos.*, 119, 8980–9002, <https://doi.org/10.1002/2014JD021861>, 2014.
- Jiang, Y., Lu, Z., Liu, X., Qian, Y., Zhang, K., Wang, Y., and Yang, X.-Q.: Impacts of global open-fire aerosols on direct radiative, cloud and surface-albedo effects simulated with CAM5, *Atmos. Chem. Phys.*, 16, 14805–14824, <https://doi.org/10.5194/acp-16-14805-2016>, 2016.
- Kaufman, Y. J., Koren, I., Remer, L. A., Rosenfeld, D., and Rudich, Y.: The effect of smoke, dust, and pollution aerosol on shallow cloud development over the Atlantic Ocean, *P. Natl. Acad. Sci. USA*, 102, 11207–11212, 2005.
- Keil, A. and Haywood, J. M.: Solar radiative forcing by biomass burning aerosol particles during SAFARI 2000: A case study based on measured aerosol and cloud properties, *J. Geophys. Res.*, 108, 8467, <https://doi.org/10.1029/2002JD002315>, 2003.
- Kolusu, S. R., Marsham, J. H., Mulcahy, J., Johnson, B., Dunning, C., Bush, M., and Spracklen, D. V.: Impacts of Amazonia biomass burning aerosols assessed from short-range weather forecasts, *Atmos. Chem. Phys.*, 15, 12251–12266, <https://doi.org/10.5194/acp-15-12251-2015>, 2015.
- Kooperman, G. J., Pritchard, M. S., Ghan, S. J., Wang, M., Somerville, R. C., and Russell, L. M.: Constraining the influence of natural variability to improve estimates of global aerosol indirect effects in a nudged version of the Community Atmosphere Model 5, *J. Geophys. Res.*, 117, D23204, <https://doi.org/10.1029/2012JD018588>, 2012.
- Korontzi, S., McCarty, J., Loboda, T., Kumar, S., and Justice, C.: Global distribution of agricultural fires in croplands from 3 years of Moderate Resolution Imaging Spectroradiometer (MODIS) data, *Global Biogeochem. Cy.*, 20, GB2021, <https://doi.org/10.1029/2005GB002529>, 2006.
- Lin, N.-H., Tsay, S.-C., Maring, H. B., Yen, M.-C., Sheu, G.-R., Wang, S.-H., Chi, K. H., Chuang, M.-T., Ou-Yang, C.-F., and Fu, J. S.: An overview of regional experiments on biomass burning aerosols and related pollutants in Southeast Asia: From BASE-ASIA and the Dongsha Experiment to 7-SEAS, *Atmos. Environ.*, 78, 1–19, 2013.
- Liu, X., Easter, R. C., Ghan, S. J., Zaveri, R., Rasch, P., Shi, X., Lamarque, J.-F., Gettelman, A., Morrison, H., Vitt, F., Conley, A., Park, S., Neale, R., Hannay, C., Ekman, A. M. L., Hess, P., Mahowald, N., Collins, W., Iacono, M. J., Bretherton, C. S., Flanner, M. G., and Mitchell, D.: Toward a minimal representation of aerosols in climate models: description and evaluation in the Community Atmosphere Model CAM5, *Geosci. Model Dev.*, 5, 709–739, <https://doi.org/10.5194/gmd-5-709-2012>, 2012.
- Lu, Z. and Sokolik, I. N.: The effect of smoke emission amount on changes in cloud properties and precipitation: A case study of Canadian boreal wildfires of 2007, *J. Geophys. Res.-Atmos.*, 118, 11777–11793, <https://doi.org/10.1002/2013JD019860>, 2013.
- Magi, B. I., Rabin, S., Shevliakova, E., and Pacala, S.: Separating agricultural and non-agricultural fire seasonality at regional scales, *Biogeosciences*, 9, 3003–3012, <https://doi.org/10.5194/bg-9-3003-2012>, 2012.
- Malm, W. C., Schichtel, B. A., Pitchford, M. L., Ashbaugh, L. L., and Eldred, R. A.: Spatial and monthly trends in speciated fine particle concentration in the United States, *J. Geophys. Res.*, 109, D03306, <https://doi.org/10.1029/2003JD003739>, 2004.
- Mlawer, E. J., Taubman, S. J., Brown, P. D., Iacono, M. J., and Clough, S. A.: Radiative transfer for inhomogeneous atmospheres: RRTM, a validated correlated-k model for the longwave, *J. Geophys. Res.*, 102, 16663–16682, 1997.
- Morrison, H. and Gettelman, A.: A new two-moment bulk stratiform cloud microphysics scheme in the Community Atmosphere Model, version 3 (CAM3). Part I: Description and numerical tests, *J. Climate*, 21, 3642–3659, 2008.
- Mu, M., Randerson, J., van der Werf, G., Giglio, L., Kasibhatla, P., Morton, D., Collatz, G., DeFries, R., Hyer, E., and Prins, E.: Daily and hourly variability in global fire emissions and consequences for atmospheric model predictions of carbon monoxide, *J. Geophys. Res.*, 116, D24303, <https://doi.org/10.1029/2011JD016245>, 2011.
- Neale, R. B., Richter, J. H., and Jochum, M.: The impact of convection on ENSO: From a delayed oscillator to a series of events, *J. Climate*, 21, 5904–5924, 2008.
- Park, S. and Bretherton, C. S.: The University of Washington shallow convection and moist turbulence schemes and their impact

- on climate simulations with the Community Atmosphere Model, *J. Climate*, 22, 3449–3469, 2009.
- Randerson, J., Chen, Y., Werf, G., Rogers, B., and Morton, D.: Global burned area and biomass burning emissions from small fires, *J. Geophys. Res.*, 117, G04012, <https://doi.org/10.1029/2012JG002128>, 2012.
- Reddington, C., Yoshioka, M., Balasubramanian, R., Ridley, D., Toh, Y., Arnold, S., and Spracklen, D.: Contribution of vegetation and peat fires to particulate air pollution in Southeast Asia, *Environ. Res. Lett.*, 9, 094006, <https://doi.org/10.1088/1748-9326/9/9/094006>, 2014.
- Richter, J. H. and Rasch, P. J.: Effects of convective momentum transport on the atmospheric circulation in the Community Atmosphere Model, version 3, *J. Climate*, 21, 1487–1499, 2008.
- Rubin, J. I., Reid, J. S., Hansen, J. A., Anderson, J. L., Collins, N., Hoar, T. J., Hogan, T., Lynch, P., McLay, J., Reynolds, C. A., Sessions, W. R., Westphal, D. L., and Zhang, J.: Development of the Ensemble Navy Aerosol Analysis Prediction System (ENAAAPS) and its application of the Data Assimilation Research Testbed (DART) in support of aerosol forecasting, *Atmos. Chem. Phys.*, 16, 3927–3951, <https://doi.org/10.5194/acp-16-3927-2016>, 2016.
- Sena, E. T., Artaxo, P., and Correia, A. L.: Spatial variability of the direct radiative forcing of biomass burning aerosols and the effects of land use change in Amazonia, *Atmos. Chem. Phys.*, 13, 1261–1275, <https://doi.org/10.5194/acp-13-1261-2013>, 2013.
- Smirnov, A., Holben, B., Eck, T., Dubovik, O., and Slutsker, I.: Cloud-screening and quality control algorithms for the AERONET database, *Remote Sens. Environ.*, 73, 337–349, 2000.
- Stier, P., Schutgens, N. A. J., Bellouin, N., Bian, H., Boucher, O., Chin, M., Ghan, S., Huneeus, N., Kinne, S., Lin, G., Ma, X., Myhre, G., Penner, J. E., Randles, C. A., Samsat, B., Schulz, M., Takemura, T., Yu, F., Yu, H., and Zhou, C.: Host model uncertainties in aerosol radiative forcing estimates: results from the AeroCom Prescribed intercomparison study, *Atmos. Chem. Phys.*, 13, 3245–3270, <https://doi.org/10.5194/acp-13-3245-2013>, 2013.
- Tarasova, T., Gorchakova, I., Sviridenkov, M., Anikin, P., and Romashova, E.: Estimation of the radiative forcing of smoke aerosol from radiation measurements at the Zvenigorod scientific station in the summer of 2002, *Izv. Atmos. Ocean. Phys.*, 40, 454–463, 2004.
- Ten Hoeve, J. E., Jacobson, M. Z., and Remer, L. A.: Comparing results from a physical model with satellite and in situ observations to determine whether biomass burning aerosols over the Amazon brighten or burn off clouds, *J. Geophys. Res.*, 117, D08203, <https://doi.org/10.1029/2011JD016856>, 2012.
- Tosca, M. G., Randerson, J. T., and Zender, C. S.: Global impact of smoke aerosols from landscape fires on climate and the Hadley circulation, *Atmos. Chem. Phys.*, 13, 5227–5241, <https://doi.org/10.5194/acp-13-5227-2013>, 2013.
- Twomey, S.: The influence of pollution on the shortwave albedo of clouds, *J. Atmos. Sci.*, 34, 1149–1152, 1977.
- van der Werf, G. R., Randerson, J. T., Giglio, L., Collatz, G. J., Mu, M., Kasibhatla, P. S., Morton, D. C., DeFries, R. S., Jin, Y., and van Leeuwen, T. T.: Global fire emissions and the contribution of deforestation, savanna, forest, agricultural, and peat fires (1997–2009), *Atmos. Chem. Phys.*, 10, 11707–11735, <https://doi.org/10.5194/acp-10-11707-2010>, 2010.
- Wan, H., Rasch, P. J., Zhang, K., Qian, Y., Yan, H., and Zhao, C.: Short ensembles: an efficient method for discerning climate-relevant sensitivities in atmospheric general circulation models, *Geosci. Model Dev.*, 7, 1961–1977, <https://doi.org/10.5194/gmd-7-1961-2014>, 2014.
- Ward, D. S., Kloster, S., Mahowald, N. M., Rogers, B. M., Randerson, J. T., and Hess, P. G.: The changing radiative forcing of fires: global model estimates for past, present and future, *Atmos. Chem. Phys.*, 12, 10857–10886, <https://doi.org/10.5194/acp-12-10857-2012>, 2012.
- Wu, L., Su, H., and Jiang, J. H.: Regional simulations of deep convection and biomass burning over South America: 2. Biomass burning aerosol effects on clouds and precipitation, *J. Geophys. Res.*, 116, D17209, <https://doi.org/10.1029/2011JD016106>, 2011.
- Zamora, L. M., Kahn, R. A., Cubison, M. J., Diskin, G. S., Jimenez, J. L., Kondo, Y., McFarquhar, G. M., Nenes, A., Thornhill, K. L., Wisthaler, A., Zelenyuk, A., and Ziemba, L. D.: Aircraft-measured indirect cloud effects from biomass burning smoke in the Arctic and subarctic, *Atmos. Chem. Phys.*, 16, 715–738, <https://doi.org/10.5194/acp-16-715-2016>, 2016.
- Zeng, T. and Wang, Y.: Nationwide summer peaks of OC / EC ratios in the contiguous United States, *Atmos. Environ.*, 45, 578–586, 2011.
- Zhang, F., Wang, J., Ichoku, C., Hyer, E. J., Yang, Z., Ge, C., Su, S., Zhang, X., Kondragunta, S., and Kaiser, J. W.: Sensitivity of mesoscale modeling of smoke direct radiative effect to the emission inventory: a case study in northern sub-Saharan African region, *Environ. Res. Lett.*, 9, 075002, <https://doi.org/10.1088/1748-9326/9/7/075002>, 2014.
- Zhang, G. J. and McFarlane, N. A.: Sensitivity of climate simulations to the parameterization of cumulus convection in the Canadian Climate Centre general circulation model, *Atmos. Ocean*, 33, 407–446, 1995.
- Zhang, J., Reid, J. S., Westphal, D. L., Baker, N. L., and Hyer, E. J.: A system for operational aerosol optical depth data assimilation over global oceans, *J. Geophys. Res.*, 113, D10208, <https://doi.org/10.1029/2007JD009065>, 2008.
- Zhang, K., Wan, H., Liu, X., Ghan, S. J., Kooperman, G. J., Ma, P.-L., Rasch, P. J., Neubauer, D., and Lohmann, U.: Technical Note: On the use of nudging for aerosol–climate model intercomparison studies, *Atmos. Chem. Phys.*, 14, 8631–8645, <https://doi.org/10.5194/acp-14-8631-2014>, 2014.
- Zhang, Z., Meyer, K., Yu, H., Platnick, S., Colarco, P., Liu, Z., and Oreopoulos, L.: Shortwave direct radiative effects of above-cloud aerosols over global oceans derived from 8 years of CALIOP and MODIS observations, *Atmos. Chem. Phys.*, 16, 2877–2900, <https://doi.org/10.5194/acp-16-2877-2016>, 2016.